THE JOURNAL OF PHYSICAL CHEMISTRY B

ARTICLE

pubs.acs.org/JPCB

Dielectric Fluctuations over Polymer Films Detected Using an Atomic Force Microscope

Nikolas Hoepker,[†] Swapna Lekkala,[‡] Roger F. Loring,[‡] and John A. Marohn*[,‡]

[†]Laboratory of Atomic and Solid State Physics, and [‡]Department of Chemistry and Chemical Biology, Cornell University, Ithaca, New York 14853, United States

Supporting Information

ABSTRACT: We present a systematic study of the frequency noise experienced by a charged atomic force microscope cantilever due to thermal dielectric fluctuations in a thin-film sample of poly(vinyl acetate). Here, the tip of the commercial atomic force microscope cantilever oscillates in the conventional direction, normal to the surface of the film, complementing our previous studies of dielectric fluctuations carried out using an ultrasensitive custom-fabricated cantilever oscillating parallel to the film surface. We show that frequency noise induced by mechanical vibrations can be distinguished from frequency noise resulting from thermal dielectric fluctuations by the dependence on applied voltage and tip-sample separation, allowing molecular information to be unambiguously extracted. A linear response theory for cantilever frequency noise over a molecular material correctly reproduces the observed dependences on frequency, voltage, and tip-sample separation. The technique is shown to measure primarily fluctuations in the electric field gradient over the surface, which in these measurements are generated by orientational relaxation of polar polymer segments.

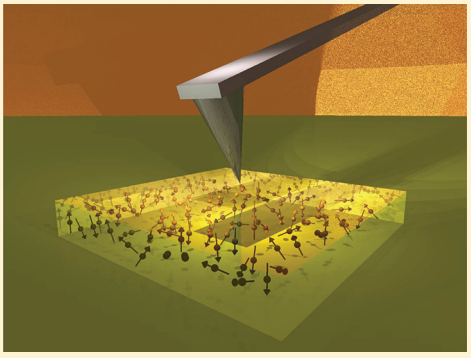

INTRODUCTION

Scanned probe microscopy has enabled the nanometer-resolution imaging of surfaces with contrast based on topography,[1] chemical forces,[1−3] magnetization,[2,4] capacitance,[5,6] and electrostatic potential.[5,7] Fluctuations in sample properties are detectable in a scanned probe experiment, according to the fluctuation-dissipation theorem, through the measurement of sample-induced cantilever dissipation. A charged Atomic Force Microscope (AFM) cantilever has been used to observe dissipation due to free and trapped carriers in semiconductors,[8−11] atomic defect motion at metal and semiconductor surfaces,[12] and image currents in metals.[13−15] A magnetic-tipped AFM cantilever has been used to probe dissipation associated with domain wall motion in ferromagnets,[16,17] eddy currents in metals,[18,19] and thermomagnetic fluctuations in submicron magnetic particles.[20,21] Sample fluctuations also give rise to stochastic force gradients and, thereby, cantilever frequency noise. Cantilever frequency noise has been used to study charge blinking in inorganic semiconductor nanoparticles[22] and generation-recombination noise in inorganic semiconductor heterojunctions.[23] In order to study the cooperativity of molecular motion near the glass transition, Israeloff and co-workers introduced the use of the charged tip of an AFM cantilever to observe electric polarization fluctuations in a thin polymer film.[24−29] In these experiments a polymer sample is spun onto a conducting substrate, and the cantilever oscillates with its body parallel to the surface and its tip parallel to the sample's surface normal: the usual AFM geometry. The sample's polarization fluctuations lead to observable cantilever frequency noise which, they proposed, could be understood by considering the interaction of the charged cantilever tip with voltage fluctuations arising from the sample.

Motivated by measurements of attonewton forces near surfaces,[30] Kuehn et al. examined the force noise induced by thermal dielectric fluctuations in a thin polymer film acting on a charged cantilever.[31,32] In these experiments, carried out with a custom-fabricated high-compliance silicon cantilever,[33,34] the cantilever body is oriented parallel to the sample's surface normal and the cantilever tip maintains a nearly constant tip-sample separation as the cantilever oscillates. A linear-response theory was developed which quantitatively predicted the observed dependence of noncontact friction[31,32] and frequency noise[35,36] on the sample's complex dielectric function, the sample thickness, and the tip-sample separation. A key finding of this analysis was that, within a point charge model for the tip, frequency noise arises from a coupling of the cantilever's tip charge with electric field gradient fluctuations generated by the sample.

Here we extend our previous analysis[35,36] of the interaction of a charged AFM tip with a dielectric surface to the case in which the tip moves perpendicular to the surface in the usual AFM geometry. In contrast to the case in which the tip moves parallel to the surface, we find that computing the cantilever frequency noise requires determining auto- and cross-correlations of stochastic fluctuations in voltage, electric field, and electric field gradient, with the dominant term containing the autocorrelation function of field gradient fluctuations. In the low-frequency limit, our analysis confirms the frequency dependence predicted by Israeloff and co-workers[24−29] but provides a complete quantitative

Received: August 2, 2011
Revised: October 6, 2011
Published: October 14, 2011

description of the dependence of the power spectrum on experimental parameters. Here we probe dielectric fluctuations over poly(vinyl acetate) in the vincinity of 1 Hz at room temperature, which have been assigned by bulk dielectric spectroscopy[37,38] and NMR spectroscopy[39] as due to orientational dynamics of the polymer backbone, the α-relaxation associated with the glass transition. We carry out systematic measurements of the power spectrum of cantilever frequency fluctuations as a function of frequency, tip-sample distance, and tip voltage using a commercial AFM cantilever over a thin poly(vinyl acetate) film. Our theory quantitatively describes these data; the only inputs to the calculation are the sample thickness, sample dielectric spectrum, and the diameter and cone angle of the cantilever tip. By connecting the information content of cantilever frequency fluctuations over a molecular sample to its dielectric spectrum, this work provides a basis for dielectric loss imaging over thin films.

EXPERIMENTAL METHODS

Scanned probe microscope measurements were performed at 0.5×10^{-6} mbar. The apparatus was not temperature controlled, but the laboratory was maintained at 20.7 °C. To reduce ambient vibrations, the scanned probe microscope was installed on a commercial vibration isolation stage (Minus-k 250BM-3) located on a vibrationally isolated cement slab. To reduce thermal drifts, the microscope's vacuum chamber was thermally insulated with styrofoam. A commercial nanopositioner (Attocube ANPz51) was used to move the cantilever with respect to the fixed sample.

A custom-built positive feedback circuit was used to drive the cantilever (MikroMasch, NSC19 Ti/Pt) at its resonance frequency of $f_c \approx 46.0$ kHz by exciting a small piezoelectric crystal to which the cantilever was affixed. The position of the cantilever was tracked with a temperature-tuned fiber-optic interferometer[40] (λ = 1310 nm), digitized, and then passed through a 20th order Butterworth bandpass filter (centered at f_c, bandwidth = 2×2000 Hz). We use a software frequency demodulator to convert the cantilever position into a frequency versus time signal (ref 35 and the Supporting Information). Frequency noise spectra were obtained from the Fourier transform of the autocorrelation function of the frequency fluctuations. The quality factor $Q \approx 2500$ was determined from ringdown measurements.

The cantilever spring constant was determined from its Brownian motion spectrum.[41] By the equipartition principle, the cantilever spring constant is given by $k_c = k_B T/\langle x_{th}^2 \rangle$. The mean-squared amplitude $\langle x_{th}^2 \rangle$ of the thermo-mechanical fluctuations was determined from 240 $\times$ 1 s position noise spectra. From these measurements, we infer a spring constant of k_c = 0.85 N/m. Irreproducibility in the location of the laser spot introduces a relative error on the order of ten percent in the k_c determination.

A polyvinyl acetate (PVAc) sample was prepared by dissolving 21.7 mg of PVAc (Sigma-Aldrich, no. 387924, used as received, MW = 140 000) in 2 mL of toluene and spin-casting at 2000 rpm for 30 s onto a gold-covered silicon substrate. After spin-casting, the sample was vacuum annealed for 12 h at 45 °C to drive off water and any remaining solvent. The resulting sample thickness and rms-roughness were h = 63 nm and h_{rms} = 1.3 nm, as measured by profilometry and atomic force microscopy, respectively.

To determine the dielectric spectrum of PVAc, a top contact of aluminum was thermally evaporated over 1.4 cm^2 of the PVAc film and electrical contact was made by silver-paint. We performed impedance measurements on the resulting capacitor using a broadband dielectric spectrometer (Turnkey Concept N40).

ANALYSIS OF FREQUENCY JITTER

The sample is represented as a continuum dielectric slab of thickness h and relative dielectric function $\varepsilon(f)$, backed by a grounded conductor at $z = -h$, and the probe is taken to move in one dimension along z, perpendicular to the polymer-vacuum interface. The probe in the absence of the applied voltage is represented by a harmonic oscillator with force constant k_c and equilibrium tip-sample distance $z = d$. The electrostatic interaction with the sample is modeled by a stochastic potential energy $W(z,t)$[42,43]

$$W(z,t) = \bar{W}(z) + \delta W(z,t) \tag{1}$$

$$\bar{W}(z) \equiv -\frac{1}{2}C(z){V_{ts}}^2 \tag{2}$$

$$\delta W(z,t) \equiv V_{ts}C(z)\delta\varphi(z_{eff},t) \tag{3}$$

Here $C(z)$ is the tip-sample capacitance, and the tip-sample voltage $V_{ts} = V_{app} - \phi_c$ is the applied voltage adjusted for the surface contact potential ϕ_c. The fluctuating potential generated by thermal motions in the sample is denoted $\delta\varphi(z,t)$, and is assumed to act on an effective point charge, equal in magnitude to the total tip charge and located at a height z_{eff} above the interface, equal to the sum of z and a constant displacement. Choices for z_{eff} are discussed below.

Expansion of $W(z,t)$ about the unperturbed equilibrium tip−sample separation $z = d$ yields a static sample-induced frequency shift $\Delta f_c(d)$ associated with $\bar{W}(z)$ and a stochastic frequency shift $\delta f_c(d,t)$ arising from $\delta W(d,t)$. To second order in $z - d$, the static frequency shift is

$$\Delta f_c(d) = \frac{f_c}{2k_c}\bar{W}_2(d) = -\frac{f_c}{4k_c}C_2(d){V_{ts}}^2 \tag{4}$$

with $\bar{W}_n(d) \equiv \mathrm{d}^n\bar{W}(z)/\mathrm{d}z^n|_{z=d}$ and $C_n(d) \equiv \mathrm{d}^nC(z)/\mathrm{d}z^n|_{z=d}$. To fourth order in $z - d$, the fluctuating frequency shift induced by probe-sample interactions is

$$\delta f_c(d,t) = \frac{f_c}{2k_c}[\delta W_2(d,t) + {k_c}^{-1}(\bar{W}_3(d)\delta W_1(d,t) + \bar{W}_1(d)\delta W_3(d,t)) - \frac{5z_{rms}^2}{6}\bar{W}_3(d)\delta W_3(d,t) + \frac{z_{rms}^2}{4}\delta W_4(d,t)] \tag{5}$$

The term containing δW_2 arises from the harmonic approximation to $\delta W(z,t)$ in eq 3. The two terms containing products of components of W_1 and W_3 arise from the interplay between cubic anharmonicity in $W(z,t)$ and the shift in equilibrium oscillator displacement caused by terms linear in $z - d$. The term quadratic in components of W_3 is the frequency shift of a cubically perturbed harmonic oscillator, calculated to second order in perturbation theory[44] within an adiabatic approximation in which the potential energy fluctuations $\delta W_3(d,t)$ are taken to be slow with respect to the period of the oscillator. This adiabatic approximation is appropriate here, as the frequency jitter occurs on time scales 4 orders of magnitude smaller than the cantilever period. This term results from calculating the frequency shift for time-independent potential anharmonicity W_3 and replacing this quantity with the slowly varying $W_3(d,t)$. The term in eq 5

proportional to δW_4 is calculated within the same adiabatic approximation to first order in perturbation theory for a quartically perturbed harmonic oscillator.[45] These two terms are proportional to z_{rms}^2, the mean-squared displacement of the cantilever from its equilibrium position.

As shown in Figure 3 below, the measured sample-induced frequency noise is quadratic in V_{ts}, and so arises from frequency fluctuations that are linear in applied voltage. We therefore classify the contributions to the frequency fluctuation in eq 5 according to their dependence on V_{ts}. The terms containing cubic anharmonicity are proportional to ${V_{ts}}^3$ and so will not be considered further. The harmonic term and the term arising from quartic anharmonicity are both linear in V_{ts}. However, unlike the harmonic term, the quartic term is dependent on the oscillation amplitude through the factor ${z_{rms}}^2$. Although this term is not negligible for the smallest d values considered here, we reserve its treatment for the Supporting Information and for the discussion of Figure 5 below and adopt the harmonic approximation to $\delta f_c(d,t)$ in eq 5

$$\delta f_c(d,t) = \frac{f_c V_{ts}}{2k_c}(C_2(d)\delta\varphi(d_{eff},t) - 2C_1(d)\delta\mathcal{E}_z(d_{eff},t) - C(d)\delta\mathcal{E}_{zz}(d_{eff},t)) \quad (6)$$

with $\delta\mathcal{E}_z(z,t) \equiv -\partial\delta\varphi(z,t)/\partial z$ the fluctuation of the electric field component along the probe coordinate and $\delta\mathcal{E}_{zz}(z,t) \equiv -\partial^2\delta\varphi(z,t)/\partial z^2$ the fluctuation in electric field gradient. The coordinate of the effective point charge z_{eff} at $z = d$ is denoted d_{eff}.

The power spectrum of cantilever frequency fluctuations is defined as

$$P_{\delta f_c}(f) \equiv P_{f_c,f_c}(f) \quad (7)$$

$$P_{A,B}(f) \equiv 4\int_0^\infty dt\, \cos(2\pi ft)\langle\delta A(d,t)\delta B(d,0)\rangle \quad (8)$$

with the angle brackets denoting a stochastic average over the fluctuating electrostatic potential and A and B representing two fluctuating quantities associated with tip-sample distance d. In eq 6, the probe frequency fluctuation is expressed as the sum of terms proportional to the electrostatic potential, to the electric field, and to the electric field gradient. Substitution into eq 8 yields equilibrium auto- and cross-correlation functions of these quantities

$$P_{\delta f_c}(f) = \left(\frac{f_c V_{ts}}{2k_c}\right)^2 [{C_2}^2(d)P_{\delta\varphi}(f) - 4C_1(d)C_2(d)P_{z,\varphi}(f) - 2C(d)C_2(d)P_{\varphi,zz}(f) + 4{C_1}^2(d)P_{z,z} - 4C(d)C_1(d)P_{z,zz}(f) + C^2(d)P_{zz,zz}(f)] \quad (9)$$

In eq 9 the subscripts z and zz refer respectively to $\delta\mathcal{E}_z$ and $\delta\mathcal{E}_{zz}$.

Evaluation of the power spectrum in eq 9 requires the calculation of equilibrium correlation functions involving the potential, the electric field, and the electric field gradient as functions of distance above the sample surface in the absence of the charged probe. Our previous studies of noncontact friction[31,32] and frequency jitter[35,36] with a probe oscillating parallel to the surface required the calculation of autocorrelation functions of $\delta\mathcal{E}_x$ and $\delta\mathcal{E}_{xx}$. These quantities were determined from linear response theory together with either of two equivalent approaches: a quasistatic approximation to electrodynamics[31,32,35,36] or a full electrodynamic calculation[35] in the limit $c \to \infty$. Here we employ the quasistatic approximation of refs 31, 32, and 35. We consider the sample in the absence of the probe, but with a fictitious time-varying point charge $q(t)$ at a distance z_1 above the interface. This perturbing charge is an artifice chosen because it couples to the fluctuating electrostatic potential generated by the sample $\varphi(z,t)$. Classical mechanical linear response theory yields the following relation between the mean electrostatic potential at another location z_2, the magnitude and frequency-dependence of the perturbing point charge, and the correlation function of electrostatic potential fluctuations at different locations

$$P_{\delta\varphi}(z_1,z_2,f) \equiv 4\int_0^\infty dt\, \cos(2\pi ft)\langle\delta\varphi(z_1,t)\delta\varphi(z_2,0)\rangle \quad (10)$$

$$P_{\delta\varphi}(z_1,z_2,f) = \frac{-4k_B T}{2\pi f}\,\mathrm{Im}\left(\frac{\tilde{\phi}(z_2,f)}{\tilde{q}(z_1,f)}\right) \quad (11)$$

$$\tilde{\phi}(z,f) \equiv \int_0^\infty dt\, e^{-i2\pi ft}\langle\varphi(z,t)\rangle \quad (12)$$

The autocorrelation function $P_{\delta\varphi}(f)$ in eq 9 represents the more general correlation function in eq 10 at $z_1 = z_2 = d_{eff}$. The mean potential $\tilde{\phi}(z_2, f)$ in eq 11 is then calculated in terms of the perturbing charge $\tilde{q}(z_1, f)$ from the quasistatic approximation to macroscopic electrodynamics for a linear dielectric using the method of images to yield an explicit expression for the power spectrum of potential fluctuations

$$P_{\delta\varphi}(z_1,z_2,f) = \frac{4k_B T\zeta''(f)}{(4\pi\varepsilon_0)2\pi f}L_0(z_1,z_2,f) \quad (13)$$

$$L_n(z_1,z_2,f) = \int_0^\infty ds\, s^n e^{-s(z_1+z_2)}\left(\frac{1-e^{-4sh}}{|1+\zeta e^{-2sh}|^2}\right) \quad (14)$$

$$\zeta(f) = \frac{\varepsilon(f)-1}{\varepsilon(f)+1} = \zeta'(f) + i\zeta''(f) \quad (15)$$

The correlation functions required for eq 9 may then be computed from eq 13 by taking coordinate derivatives, e.g.

$$P_{zz,zz}(f) = \frac{\partial^4}{\partial^2 z_1 \partial^2 z_2}P_{\varphi,\varphi}(z_1,z_2,f)|_{z_1=z_2=d_{eff}} \quad (16)$$

The jitter spectrum is then given by

$$P_{\delta f_c}(f) = \frac{{f_c}^2{V_{ts}}^2}{{k_c}^2}\frac{k_B T\zeta''(f)}{2\pi(4\pi\varepsilon_0)f}\{{C_2}^2(d)K_0 - 4C_2(d)C_1(d)K_1 + (2C_2(d)C(d) + 4{C_1}^2(d))K_2 - 4C(d)C_1(d)K_3 + C^2(d)K_4\} \quad (17)$$

with

$$K_m \equiv L_m(z_1,z_2,f)|_{z_1=z_2=d_{eff}} \quad (18)$$

The power spectrum of probe frequency fluctuations arising from electrostatic interactions with the sample is seen in eq 17 to contain contributions from a variety of dynamical correlations. As shown in eq 6, the terms proportional to ${C_2}^2$, ${C_1}^2$, and C^2 are associated respectively with autocorrelations of fluctuations in electrostatic potential, electric field, and electric field gradient. The remaining terms derive from cross-correlations among these fluctuations. In our previous study of ultrasensitive cantilevers

oscillating parallel to the sample surface,[36] only the autocorrelation function of field gradient fluctuations contributed to the probe frequency jitter, since the capacitance could be assumed to remain constant over the course of the cantilever period.[36]

Unlike the spectrum of polymer-induced cantilever frequency noise, the spectrum of frequency noise originating in cantilever thermo-mechanical position fluctuations is independent of frequency and given by[35,36,46,47]

$$P_{\delta f_c}^{\mathrm{therm}}(f) = \frac{k_B T f_c}{2\pi x_{\mathrm{rms}}^2 k_c Q} \tag{19}$$

where x_{rms} = 32 nm is the root-mean-squared cantilever amplitude in our experiments.

In order to analyze the contribution to measured probe frequency jitter from external mechanical vibrations, we add to the equilibrium tip-sample separation d a stochastic fluctuation $\delta d_{\mathrm{ex}}(d,t)$. Making this substitution in eq 4 and linearizing in $\delta d_{\mathrm{ex}}(d,t)$ gives a frequency fluctuation which depends on cubic anharmonicity and which is quadratic in applied voltage.

$$\begin{aligned}\delta f_{\mathrm{ex}}(d,t) &= \bar{W}_3(d)\delta d_{\mathrm{ex}}(d,t)\\ &= -\frac{1}{2}C_3(d){V_{\mathrm{ts}}}^2\delta d_{\mathrm{ex}}(d,t)\end{aligned} \tag{20}$$

Since these fluctuations are uncorrelated with the dielectric fluctuations considered previously, we can separately determine the contribution to the power spectrum from external vibrations to be proportional to the power spectrum of mechanical fluctuations in d

$$P_{\delta f_{\mathrm{ex}}}(f) = \left(\frac{f_c C_3(d){V_{\mathrm{ts}}}^2}{4k_c}\right)^2 P_{\delta d_{\mathrm{ex}}}(f) \tag{21}$$

The validity of this expression is assessed in the discussion of Figure 3B.

Evaluating the jitter power spectrum from dielectric fluctuations in eq 17 or from mechanical noise in eq 21 requires knowledge of the tip-sample capacitance $C(d)$ and its derivatives. We model $C(d)$ by representing the tip as the superposition of a cone and a sphere.[48] The contribution of the cone is discussed in the Supporting Information and in connection with Figure 4 below. As shown in the Supporting Information, the cone does not contribute significantly to the calculated jitter. The contribution of the sphere is discussed here. A sphere of radius R representing the probe tip is centered at height $d + R$ over a dielectric film of thickness h and dielectric constant $\varepsilon_0\varepsilon_r$. The capacitance is given by an approximation that we have employed previously[35]

$$\begin{aligned}C(d) &= 4\pi\varepsilon_0 R\sum_{n=1}^{\infty}\frac{\sinh\alpha}{\sinh n\alpha}\\ \alpha &= \cosh^{-1}\left[1+\frac{d}{R}+\frac{h}{\varepsilon_r R}\right]\end{aligned} \tag{22}$$

For this geometry, the image charges within the sphere are located at heights z with $d < z < d + R$. The coordinate of the effective point charge, discussed above, can be assigned to lie in this range. In calculations below, we compare the consequences of employing the two extremes, $d_{\mathrm{eff}} = d$ and $d_{\mathrm{eff}} = d + R$.

Israeloff and co-workers[24−29] interpreted their measurements of cantilever frequency fluctuations over polymer films in terms of voltage fluctuations driven by polarization fluctuations in the sample. We next compare their analysis to our results given here. Their analysis is based on two steps: the relation of cantilever frequency fluctuations to voltage fluctuations, and the determination of voltage fluctuations from linear response theory. The power spectrum of cantilever frequency fluctuations is related to that of voltage fluctuations by eq 2 of ref 25, which in our notation is

$$P_{\delta f_c}(f) = \left(\frac{\partial\Delta f_c(d)}{\partial V_{\mathrm{ts}}}\right)^2 P_{\delta\varphi}(f) \tag{23}$$

with $\Delta f_c(d)$ the static cantilever frequency shift in eq 4. The result in ref 25 includes on the right-hand side of the equality a dimensionless factor G stated to be of order unity, which is omitted here. The power spectrum of voltage fluctuations is then related to the complex capacitance by eq 2 of ref 49, which in our notation is

$$P_{\delta\varphi}(f) = -\frac{4k_B T}{2\pi f}\,\mathrm{Im}\left(\frac{1}{\tilde{C}(f)}\right) \tag{24}$$

We evaluate these two expressions for the point charge model of sample-tip interactions that we employ here. Our linear response expression in eq 11, when evaluated at $z_1 = z_2 = d_{\mathrm{eff}}$ contains the voltage to charge ratio $\tilde{\varphi}(d_{\mathrm{eff}}, f)/\tilde{q}(d_{\mathrm{eff}}, f)$. Equating this ratio to the inverse of the complex capacitance $1/\tilde{C}(f)$ reduces our eq 11 to eq 24. Substituting this result into eq 23 and evaluating the voltage derivative with eq 4 gives

$$P_{\delta f_c}(f) = \left(\frac{f_c V_{\mathrm{ts}}}{2k_c}\right)^2 {C_2}^2(d)P_{\delta\varphi}(f) \tag{25}$$

which is the first term in our eq 9. However our result in eq 9 also includes contributions to the jitter power spectrum from auto- and cross-correlations from fluctuations in electric field and electric field gradients. We show below in comparing this prediction to measurements that the contribution of the voltage fluctuations in eq 25 is small compared to other terms in eq 9. Our analysis is based on the same basic physical picture employed by Israeloff et al.[24−29] that cantilever frequency fluctuations are driven by dielectric fluctuations in the sample. However, our treatment generalizes the implicit assumption in eq 23 that in the limit of a point charge interaction, the tip couples only to fluctuations in electrostatic potential by including the coupling to fluctuations in gradients of the potential.

RESULTS AND DISCUSSION

In Figure 2, we show the observed frequency noise spectra over PVAc for tip-sample distances d = 90 and 240 nm and for a range of tip voltages from −4 to +4 V. Each of the frequency noise spectra in Figure 2 is generated by averaging 20 frequency transients, each lasting 5 s. The spectra show three distinct features: a $1/f$ component at low frequencies, spikes near 25 Hz, and a regime proportional to f^2 at large frequencies. The latter, which is only significant beyond 10 Hz, stems from noise in our instrumentation, primarily noise in the photodetector, and does not interfere with measurements of the frequency noise spectrum below 10 Hz. We are able to attribute this noise to our instrumentation because of its characteristic $\propto f^2$ frequency dependence,[35,46,47] and because it is independent of both tip-sample distance and tip voltage. By contrast, both the spikes near

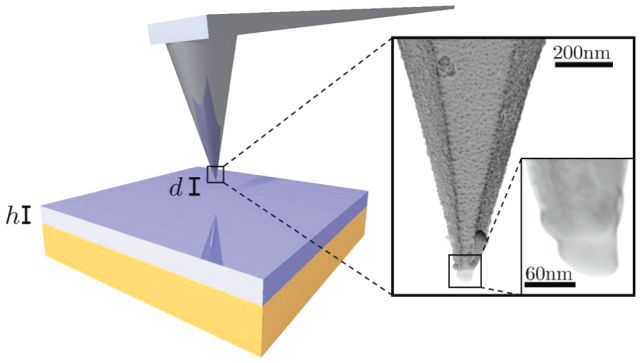

Figure 1. Charged cantilever tip is positioned a distance d above a dielectric sample of thickness h. Inset: A scanning electron microscope (SEM) image of the cantilever tip, from which we infer a tip radius of 40 nm.

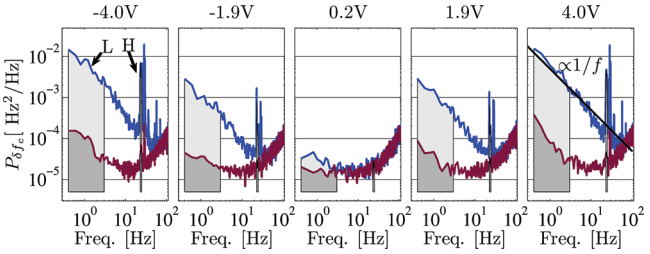

Figure 2. Frequency noise spectra for tip voltages ranging from −4 to +4 V and tip-sample distances of d = 90 (upper line) and 240 nm (lower line). Each spectrum was generated by averaging 20 frequency transients, each lasting 5 s. A $1/f$ guideline is shown.

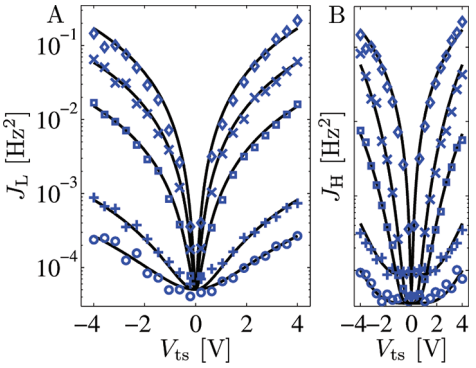

Figure 3. Frequency noise spectra in Figure 2 integrated from 0.4 to 3 Hz (A) and 23 to 25 Hz (B) as a function of tip voltage at various tip−sample separations (50 nm, ◇; 62 nm, ×; 90 nm, □; 180 nm, +; 240 nm, ○). Continuous curves are fits to $\propto V_{ts}^2$ (A) and $\propto V_{ts}^4$ (B), plus a noise floor.

25 Hz and the $1/f$ portion of the noise depend on the tip voltage and increase with increasing proximity to the sample. We conclude that these two sources of noise originate from an electrostatic tip-sample interaction. To quantify their voltage dependence, we integrate the power spectra in Figure 2 over a well-defined frequency bandwidth. The result of this integration is a mean-squared frequency noise, which we shall henceforth call jitter. In Figure 3 we show jitter as a function of tip voltage for a range of tip-sample distances. In Figure 3A we have integrated over the $1/f$ portion of the spectrum (0.4−3 Hz), whereas in Figure 3B we have integrated over the noise spikes (23−25 Hz). The jitter in these frequency regimes, which we designate as J_L for the $1/f$ regime and J_H for the noise spikes, respectively, shows different voltage dependence. While J_L in Figure 3A scales as V_{ts}^2, a quartic voltage dependence V_{ts}^4 of J_H is shown in Figure 3B. In both panels of Figure 3, the respective voltage dependence is maintained for tip-sample distances ranging from 50 to 240 nm, a range over which jitter changes by 3 orders of magnitude. We conclude that there are two distinct processes responsible for the observed frequency noise in Figures 2 and 3.

The quartic voltage dependence in Figure 3B suggests that the frequency noise is induced by stage vibrations as predicted in eq 21. To verify this interpretation, we measured the stage vibration spectrum, $P_{\delta d_{ex}}(f)$, by laser interferometry. The vibration noise spectrum does, in fact, also show characteristic spikes near 25 Hz (Supporting Information, Figure 2). To quantitatively test eq 21, we require the third spatial derivative of the tip-sample capacitance $C_3(d)$. Following Cherniavskaya et al.,[48] we model the cantilever tip as a cone with a sphere at its tip. The sphere capacitance is given in eq 22, and the cone capacitance is discussed in the Supporting Information. From scanning electron microscope (SEM) images as in Figure 1, we infer a tip radius of R = 40 nm. We validate the cone-sphere model by comparing the second derivative of the modeled $C(d)$ to the measured value we infer from eq 4. We extract from eq 4 the measured $C_2(d)$, using the known resonance frequency f_c, spring constant k_c, and measurements of resonance frequency as a function of tip-sample voltage. The sample induced shift in resonance frequency is negative, which implies that $C_2(d)$ in eq 4 is positive. In Figure 4, we compare $C_2(d)$ from the cone-sphere model with the measured result for various tip-sample distances. We find that for a cone half angle of 16° the measured $C_2(d)$ is in close agreement with the cone-sphere model. If we instead use the manufacturer's nominal value of 20° for the half angle, the model slightly overestimates $C_2(d)$. We attribute this disagreement to the octagonal pyramid shape of the cantilever. Because a cone half angle of 16° better reproduces the observed capacitance, we will use that angle to estimate $C_3(d)$ in eq 21 and to interpret the data in Figure 3B. The jitter data in Figure 3B can be fit to the form $J_H = cV_{ts}^4$, with c a constant. A predicted value for c can be determined from eq 21 by integrating the power spectrum $P_{\delta d_{ex}}$ from 23 to 25 Hz, and using the cone-sphere model predictions for $C_3(d)$. A comparison of the measured and predicted fit coefficients as a function of tip-sample distance is shown in the inset of Figure 4. From the data in Figure 3B, we see that eq 21 correctly predicts the distance dependence, V_{ts} dependence, frequency dependence, and magnitude of $P_{\delta f_{ex}}$. The excellent agreement further validates the accuracy of the cone-sphere model.

Having identified the origin of the higher frequency jitter in Figure 3B as mechanical vibrations and having established the validity of our capacitance model, we return to the low-frequency jitter data in Figures 2 and 3A. The observed noise at low frequencies is quadratic in voltage, as predicted by eq 17, and has a $1/f$ frequency noise spectrum.[24−27,36,50] eq 17 predicts the frequency dependence of the jitter spectrum from $\varepsilon(f)$, the complex-valued relative dielectric function. In the low frequency limit, eq 17 yields a frequency spectrum proportional to $\varepsilon''(f)/f$. Dielectric measurements of PVAc films shown in the Supporting Information (Figure 3) demonstrate that the dielectric spectrum $\varepsilon''(f)$ is nearly constant over the frequency range 0.4 to 3 Hz.

dx.doi.org/10.1021/jp207387d |J. Phys. Chem. B 2011, 115, 14493–14500

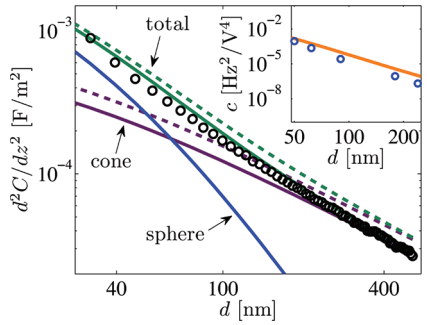

Figure 4. Measured capacitance second derivative, C_2, versus tip height (○). The solid lines are the predicted contributions from a 40 nm sphere, a cone with a half angle of 16°, and both sphere plus cone. The dashed lines show predictions for a cone angle of 20°. Inset: Fit coefficient c in $J_H = cV_{ts}^4$ from Figure 3B (circles) and prediction (line) from vibration noise determined by interferometry (Supporting Information, Figure 2).

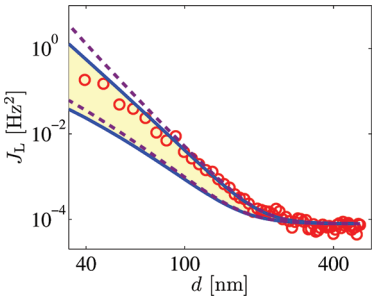

Figure 5. Measured jitter (○) as a function of tip-sample height and the prediction from integrating eq 17 (solid lines). The bottom (top) solid line is based on the assumption that all of the charge is located at the center (bottom) of the sphere. The dashed lines include contributions from anharmonic tip-sample interactions.

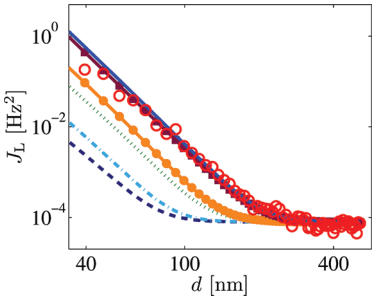

Figure 6. The jitter data (circles) and a calculation obtained by integrating eq 17 with $d_{eff} = d$ (solid curve). The contributions listed in eq 17 to the total calculated jitter are shown separately. In order of increasing magnitude they are: a term proportional to K_0 (dashed line), terms proportional to K_1 (dot-dashed line), K_2 (dotted line), K_3 (solid line with ○), and a term proportional to K_4 (solid line with □). Whereas K_0 arises from voltage fluctuations, K_1 arises from cross-correlations of the electric field and the voltage, K_2 arises from both the autocorrelation function of the electric field and cross-correlations between the electric field gradient and the voltage, K_3 arises from cross-correlations between the electric field and the electric field gradient, and K_4 is a contribution from the autocorrelation function of field gradient fluctuations. The latter is shown to be by far the dominant term, and the contribution from voltage fluctuations is shown to be negligibly small.

For this case eq 17 predicts a $1/f$ noise dependence, in agreement with the data in Figure 2. To test the distance dependence and the magnitude of the noise predicted by eq 17, we have measured jitter in a 0.4 Hz to 3 Hz bandwidth as a function of tip-sample separation d. At each distance point, we measured the resonance frequency versus voltage to determine the surface potential. We then applied a tip voltage of 3 V below the contact potential and averaged four 5s long frequency transients to obtain jitter in a 0.4 Hz to 3 Hz bandwidth. Figure 5 compares these data to the predictions of eq 17 plus a thermal noise floor from eq 19. To calculate jitter from eq 17, we require the capacitance $C(d)$ and its first two spatial derivatives $C_1(d)$ and $C_2(d)$. Figure 4 demonstrates the validity of the cone-sphere model in representing $C_2(d)$. In the Supporting Information, we treat the contribution to the jitter spectrum from the cone capacitance, and show that it is negligible. We therefore show in Figure 5 jitter calculations using only the sphere capacitance in eq 22. Evaluating eq 17 requires the dielectric function $\varepsilon(f)$, and measured values are used (Supporting Information, Figure 3). The tip-sample interaction is modeled in eq 17 by representing the tip charge as localized at a point with equilibrium tip−sample distance d_{eff}. The charge may be taken to be located between the lowest point on the tip and the sphere center, or $d < d_{eff} < d + R$. The resulting range of predictions is indicated by the shaded area in Figure 5, with the upper boundary of the shaded area indicating $d_{eff} = d$ and the lower boundary $d_{eff} = d + R$. The data are well represented by $d_{eff} \approx d$, which is most likely due to the cantilever's leading edge deviating from a spherical geometry (Figure 1). An alternative explanation is that, when summing over tip charge to compute the total jitter, the strong distance dependence of the fluctuating surface-induced potentials disproportionally weights the charges closest to the sample. The inclusion of the lowest-order anharmonic correction to this interaction, a quartic term that introduces a dependence on oscillation amplitude, is discussed in the Supporting Information. The dashed curves in Figure 5A were calculated for $d_{eff} = d$ and $d_{eff} = d + R$ from eq 4 in the Supporting Information, which includes this contribution. Anharmonicity enhances jitter at the smallest values of d, but the relative contribution to the total jitter is not large.

The jitter spectrum is decomposed in eq 9 into terms associated with auto- and cross-correlations among fluctuations in electrostatic potential, electric field, and electric field gradient. The jitter data (circles) and the calculation with $d_{eff} = d$ (solid curve) from Figure 5 are reproduced in Figure 6. Also shown in Figure 6 are the contributions listed in eq 17 to the total calculated jitter. The power spectrum of the electric field gradient fluctuations is by far the dominant term, whereas the contribution from voltage fluctuations is negligibly small. The contribution from voltage fluctuations is shown in eq 25 to result from applying to our point charge model the analysis of Israeloff and co-workers.[25,49] The contribution from voltage fluctuations in eq 25 reproduces the frequency dependence $\varepsilon''(f)/f$ of the complete jitter spectrum and has a comparable though not identical dependence on tip-sample separation. However, Figure 6 shows that this term is not the dominant contribution to the measured spectrum, which arises primarily from fluctuations in electric field gradient.

The measured jitter in Figures 5 and 6 was determined by integrating the frequency noise spectra in Figure 2 between 0.3 and 4 Hz, and the calculated jitter in Figures 5 and 6 was determined using measured dielectric spectra over the same

frequency range to compute the frequency spectrum from eqs 14, 17, and 18. The agreement between calculated and measured jitter in Figures 5 and 6 demonstrates that cantilever frequency noise over a specified frequency range reflects dielectric fluctuations in the PVAc sample over that frequency range. The calorimetric glass transition temperature of high molecular weight PVAc is 300 K,[37] so that our PVAc sample is slightly below T_g. For the particular case of PVAc below its glass transition temperature, dielectric fluctuations in the frequency range 0.3 to 4 Hz arise from the α-relaxation process,[37] whose dramatic slowing down with temperature is associated with the glass transition. These dynamics in PVAc reflect cooperative, hindered reorientational motions of the polymer backbone.[39,51] More generally, the agreement between calculated and measured jitter in Figures 5 and 6 shows that the cantilever frequency noise spectrum over a dielectric film probes the same molecular motions that contribute to the dielectric spectrum in the measured frequency range.

CONCLUSIONS

We have systematically studied the frequency, voltage, amplitude, and distance dependence of frequency noise experienced by a charged atomic force microscope cantilever over a thin poly(vinyl acetate) film. In the measurements reported here, the low frequency window in the jitter spectrum reflecting molecular motions in the sample is bounded on the high-frequency side by environmental noise but is not obscured by it. We have demonstrated that frequency noise induced by environmental vibrations can be distinguished from frequency noise induced by molecular motions based on the height and voltage dependence of the noise, permitting the unambiguous extraction of molecular information from this measurement. Other authors[24−29] have considered cantilever frequency noise due to sample voltage fluctuations, but we find that fluctuations in electric field gradients make the dominant contributions to cantilever frequency noise. Our theoretical analysis yields the relation in eq 17, which connects the power spectrum of cantilever frequency fluctuations to the frequency dependence of the sample dielectric spectrum. This relation predicts that jitter measurements over a given frequency range reflect the dynamics that give rise to the dielectric spectrum over that same frequency range. Our measurements of the jitter spectrum in the neighborhood of 1 Hz probe the dynamics reflected in the dielectric spectrum of poly (vinyl acetate) in this frequency regime. This frequency range for this material at room temperature is associated with the orientational dynamics of polar polymer segments, the α-relaxation associated with the glass transition.[24−29,37] Our experimental verification of the quantitative connection between the jitter observable and dielectric relaxation suggests the application of an atomic force microscope with a commercial cantilever to spatial imaging based on dielectric relaxation. The results described here are a necessary preliminary toward using a quantitative analysis of frequency noise to address morphology, composition, and ion motion in technologically important samples such as fuel cell membranes[52−55] and bulk heterojunction solar cells.[56−60]

ASSOCIATED CONTENT

Supporting Information. Derivation of the anharmonicity correction shown as dashed curves in Figure 5, the contribution of a conical cantilever tip to the jitter spectrum, the amplitude dependence of the low frequency jitter, the external mechanical vibration noise spectrum, the observed dielectric spectrum of poly (vinyl acetate), the contact potential difference as a function of tip−sample height, and the Brownian motion position noise spectrum. This material is available free of charge via the Internet at http://pubs.acs.org.

AUTHOR INFORMATION

Corresponding Author

*E-mail: jam99@cornell.edu. Phone: +607 255 2004. Fax: +607 255 4137.

ACKNOWLEDGMENT

N.H. acknowledges the National Science Foundation through the Cornell Center for Nanoscale Systems (EEC-0117770 and EEC-0646547). J.M. acknowledges the National Science Foundation (DMR-1006633). S.L. and R.F.L acknowledge the National Science Foundation (CHE-0743299). This work was performed in part at the Cornell NanoScale Science and Technology Facility, a member of the National Nanotechnology Infrastructure Network, supported by the National Science Foundation (ECS-0335765).

REFERENCES

(1) Binnig, G.; Quate, C.; Gerber, C. *Phys. Rev. Lett.* **1986**, *56*, 930–933.
(2) Martin, Y.; Williams, C. C.; Wickramasinghe, H. K. *J. Appl. Phys.* **1987**, *61*, 4723–4729.
(3) Frisbie, C. D.; Rozsnyai, L. F.; Noy, A.; Wrighton, M. S.; Lieber, C. M. *Science* **1994**, *265*, 2071–2074.
(4) Rugar, D.; Mamin, H. J.; Guethner, P.; Lambert, S. E.; Stern, J. E.; McFadyen, I.; Yogi, T. *J. Appl. Phys.* **1990**, *68*, 1169–1183.
(5) Martin, Y.; Abraham, D. W.; Wickramasinghe, H. K. *Appl. Phys. Lett.* **1988**, *52*, 1103–1105.
(6) Kalinin, S. V.; Gruverman, A. *Scanning Probe Microscopy: Electrical and Electromechanical Phenomena at the Nanoscale*; Springer Verlag: New York, 2005.
(7) Nonnenmacher, M.; O'Boyle, M. P.; Wickramasinghe, H. K. *Appl. Phys. Lett.* **1991**, *58*, 2921–2923.
(8) Denk, W.; Pohl, D. W. *Appl. Phys. Lett.* **1991**, *59*, 2171–2173.
(9) Stowe, T. D.; Kenny, T. W.; Thomson, D. J.; Rugar, D. *Appl. Phys. Lett.* **1999**, *75*, 2785–2787.
(10) Park, J. Y.; Ogletree, D. F.; Thiel, P. A.; Salmeron, M. *Phys. Rev. B* **2007**, *76*, 064108.
(11) Qi, Y.; Park, J. Y.; Hendriksen, B. L. M.; Ogletree, D. F.; Salmeron, M. *Phys. Rev. B* **2008**, *77*, 184105.
(12) Hoffmann, P. M.; Jeffery, S.; Pethica, J. B.; Ozer, H. O.; Oral, A. *Phys. Rev. Lett.* **2001**, *87*, 265502.
(13) Dorofeyev, I.; Fuchs, H.; Wenning, G.; Gotsmann, B. *Phys. Rev. Lett.* **1999**, *83*, 2402–2405.
(14) Persson, B. N. J.; Volokitin, A. I. *Phys. Rev. Lett.* **2000**, *84*, 3504.
(15) Dorofeyev, I.; Fuchs, H.; Gotsmann, B. *Phys. Rev. Lett.* **2000**, *84*, 3505.
(16) Grütter, P.; Liu, Y.; LeBlanc, P.; Dürig, U. *Appl. Phys. Lett.* **1997**, *71*, 279.
(17) Liu, Y.; Grütter, P. *J. Appl. Phys.* **1998**, *83*, 5922–5926.
(18) Hoffmann, B.; Houbertz, R.; Hartmann, U. *Appl. Phys. A: Mater. Sci. Process.* **1998**, *66*, S409–S413.
(19) Nalladega, V.; Sathish, S.; Jata, K. V.; Blodgett, M. P. *Rev. Sci. Instrum.* **2008**, *79*, 073705.
(20) Stipe, B. C.; Mamin, H. J.; Stowe, T. D.; Kenny, T. W.; Rugar, D. *Phys. Rev. Lett.* **2001**, *86*, 2874–2877.
(21) Ng, T. N.; Jenkins, N. E.; Marohn, J. A. *IEEE Trans. Magn.* **2006**, *42*, 378–381.

(22) Krauss, T. D.; Brus, L. E. *Phys. Rev. Lett.* **1999**, *83*, 4840–4843.
(23) Cockins, L.; Miyahara, Y.; Grütter, P. *Phys. Rev. B* **2009**, *79*, 121309.
(24) Walther, L. E.; Israeloff, N. E.; Vidal Russell, E.; Alvarez Gomariz, H. *Phys. Rev. B* **1998**, *57*, R15112–R15115.
(25) Walther, L. E.; Russell, E. V.; Israeloff, N. E.; Gomariz, H. A. *Appl. Phys. Lett.* **1998**, *72*, 3223–3225.
(26) Russell, E. V.; Israeloff, N. E.; Walther, L. E.; Gomariz, H. A. *Phys. Rev. Lett.* **1998**, *81*, 1461–1464.
(27) Russell, E. V.; Israeloff, N. E. *Nature* **2000**, *408*, 695–698.
(28) Crider, P. S.; Majewski, M. R.; Zhang, J.; Ouckris, H.; Israeloff, N. E. *Appl. Phys. Lett.* **2007**, *91*, 013102.
(29) Crider, P. S.; Majewski, M. R.; Zhang, J.; Oukris, H.; Israeloff, N. E. *J. Chem. Phys.* **2008**, *128*, 044908.
(30) Stipe, B. C.; Mamin, H. J.; Stowe, T. D.; Kenny, T. W.; Rugar, D. *Phys. Rev. Lett.* **2001**, *87*, 096801.
(31) Kuehn, S.; Loring, R. F.; Marohn, J. A. *Phys. Rev. Lett.* **2006**, *96*, 156103.
(32) Kuehn, S.; Marohn, J. A.; Loring, R. F. *J. Phys. Chem. B* **2006**, *110*,
14525–145258.
(33) Stowe, T. D.; Yasumura, K.; Kenny, T. W.; Botkin, D.; Wago, K.; Rugar, D. *Appl. Phys. Lett.* **1997**, *71*, 288–290.
(34) Jenkins, N. E.; DeFlores, L. P.; Allen, J.; Ng, T. N.; Garner, S. R.; Kuehn, S.; Dawlaty, J. M.; Marohn, J. A. *J. Vac. Sci. Technol. B* **2004**, *22*, 909–915.
(35) Yazdanian, S. M.; Marohn, J. A.; Loring, R. F. *J. Chem. Phys.* **2008**, *128*, 224706.
(36) Yazdanian, S. M.; Hoepker, N.; Kuehn, S.; Loring, R. F.; Marohn, J. A. *Nano Lett.* **2009**, *9*, 2273–2279.
(37) Richert, R.; Wagner, H. *Solid State Ionics* **1998**, *105*, 167–173.
(38) Tyagi, M.; Alegra, A.; Colmenero, J. *Phys. Rev. E* **2007**, *75*, 061805.
(39) Tracht, U.; Heuer, A.; Spiess, H. W. *J. Chem. Phys.* **1999**, *111*, 3720–3727.
(40) Bruland, K. J.; Garbini, J. L.; Dougherty, W. M; Chao, S. H.; Jensen, S. E.; Sidles, J. A. *Rev. Sci. Instrum.* **1999**, *70*, 3542–3544.
(41) Hutter, J. L.; Bechhoefer, J. *Rev. Sci. Instrum.* **1993**, *64*, 1868–1873.
(42) Brau, C. A. *Modern Problems In Classical Electrodynamics*; Oxford University Press, Inc., 2004.
(43) Silveira, W. R.; Muller, E. M.; Ng, T. N.; Dunlap, D. H.; Marohn, J. A. In *Scanning Probe Microscopy: Electrical and Electromechanical Phenomena at the Nanoscale*; Kalinin, S. V., Gruverman, A., Eds.; Springer Verlag: New York, 2007; Vol. II, pp 788−830.
(44) Goldstein, H.; Poole, C. P.; Safko, J. L. *Classical Mechanics*; Addison Wesley: Menlo Park, CA, 2002; pp 545−547.
(45) Pathak, A.; Mandal, S. *Phys. Lett. A* **2001**, *286*, 261–276.
(46) Albrecht, T. R.; Grütter, P.; Horne, D.; Rugar, D. *J. Appl. Phys.* **1991**, *69*, 668–673.
(47) Obukhov, Y.; Fong, K. C.; Daughton, D.; Hammel, P. C. *J. Appl. Phys.* **2007**, *101*, 034315.
(48) Cherniavskaya, O.; Chen, L.; Weng, V.; Yuditsky, L.; Brus, L. E. *J. Phys. Chem. B* **2003**, *107*, 1525–1531.
(49) Israeloff, N. E. *Phys. Rev. B* **1996**, *53*, R11913–R11916.
(50) Israeloff, N. E.; Grigera, T. S. *Europhys. Lett.* **1998**, *43*, 308–313.
(51) McCrum, N. G.; Read, B. E.; Williams, G. *Anelastic and Dielectric Effects in Polymeric Solids*; Dover Publications Inc.: New York, 1991.
(52) Bussian, D. A.; O'Dea, J. R.; Metiu, H.; Buratto, S. K. *Nano Lett.* **2007**, *7*, 227–232.
(53) Schmidt-Rohr, K.; Chen, Q. *Nat. Mater.* **2008**, *7*, 75–83.
(54) Robertson, N. J.; Kostalik, H. A.; Clark, T. J.; Mutolo, P. F.; Abruna, H. D.; Coates, G. W. *J. Am. Chem. Soc.* **2010**, *132*, 3400–3404.
(55) O'Dea, J. R.; Buratto, S. K. *J. Phys. Chem. B* **2011**, *115*, 1014–1020.
(56) Chiesa, M.; Bürgi, L.; Kim, J. S.; Shikler, R.; Friend, R. H.; Sirringhaus, H. *Nano Lett.* **2005**, *5*, 559–563.
(57) Coffey, D. C.; Ginger, D. S. *Nat. Mater.* **2006**, *5*, 735–740.
(58) Segalman, R. A.; McCulloch, B.; Kirmayer, S.; Urban, J. J. *Macromolecules* **2009**, *42*, 9205–9216.
(59) Giridharagopal, R.; Ginger, D. S. *J. Phys. Chem. Lett.* **2010**, *1*, 1160–1169.
(60) Groves, C.; Reid, O. G.; Ginger, D. S. *Acc. Chem. Res.* **2010**, *43*, 612–620.